Image Reconstruction from Orthogonal Fourier-Mellin Moments

Xiaoyu Wang and Simon Liao

University of Winnipeg, Winnipeg, Canada
s.liao@uwinnipeg.ca

Abstract. In this research, the main sources of computational error in orthogonal Fourier-Mellin moments (OFMMs) are analyzed, and a numerical integration method under the Cartesian coordinate system is proposed to improve the accuracy of OFMMs computing. To demonstrate the improved computational accuracy, image reconstructions from higher orders of orthogonal Fourier-Mellin moments, up to 220 for both of radial and harmonic orders, are conducted.

Keywords: Orthogonal Fourier-Mellin moments, moment computing, image reconstruction.

1 Introduction

Introduced by Hu[4] in 1961, the moment methods have been utilized in applications of image analysis, pattern recognition, object classification, and many other scientific fields. We refer to books written by Mukundan and Ramakrishnan[7], Pawlak[10], and Flusser[1] as background study for the moment methods.

Sheng and Shen introduced orthogonal Fourier-Mellin moments (OFMMs) as the generalized Zernike moments in 1994[14]. Sheng and Shen showed that the performance of orthogonal Fourier-Mellin moments is superior to that of the Zernike moments in term of image reconstruction and signal-to-noise ratio. In recent years, some research progress on the computational issues of orthogonal Fourier-Mellin moments has been achieved[8][2][17][15].

In this research, we have analyzed the main sources of computational error in orthogonal Fourier-Mellin moments, and proposed an efficient method to improve the accuracy of OFMMs computing, especially for the higher order moments. With the substantially improved accurate moments, the image reconstruction from a finite set of orthogonal Fourier-Mellin moments, up to 220 for both of radial and harmonic orders, is performed with highly satisfied results.

2 Orthogonal Fourier-Mellin Moments

Sheng and Shen introduced the orthogonal Fourier-Mellin moments, which are defined in a polar coordinate system over the interior of the unit circle[14]

$$\Phi_{nm} = \frac{1}{2\pi\alpha_n} \int_0^{2\pi} \int_0^1 f(r,\theta) Q_n(r) exp(-jm\theta) r dr d\theta, \tag{1}$$

M. Kamel and A. Campilho (Eds.): ICIAR 2013, LNCS 7950, pp. 687–694, 2013.

where $f(r,\theta)$ is an image function, the circular harmonic order $m = 0, \pm 1, \pm 2$, ..., and

$$\alpha_n = \frac{1}{2(n+1)} \tag{2}$$

is a normalization constant. The polynomials $Q_n(r)$are

$$Q_n(r) = \sum_{s=0}^{n} \alpha_{ns} r^s, \tag{3}$$

where

$$\alpha_{ns} = (-1)^{n+s} \frac{(n+s+1)!}{(n-s)!s!(s+1)!} \tag{4}$$

are called coefficients of the nth polynomial with n starting from zero.

Since the set of $Q_n(r)$ is orthogonal over the range $0 \leq r \leq 1$:

$$\int_0^1 Q_n(r) Q_k(r) r dr = \alpha_n \delta_{nk}, \tag{5}$$

where δ_{nk} is the Kronrcker symbol, the basis functions $Q_n(r)exp(-jm\theta)$ in (1) are orthogonal over the unit circle.

The orthogonality of the set $Q_n(r)exp(-jm\theta)$ allows us to reconstruct an image function defined in the unit circle by the inverse orthogonal Fourier-Mellin transform

$$f(r,\theta) = \sum_{n=0}^{\infty} \sum_{m=-\infty}^{\infty} \Phi_{nm} Q_n(r) exp(jm\theta). \tag{6}$$

In practice, with a finite set of orthogonal Fourier-Mellin moments Φ_{nm}, where $-M_{max} \leq m \leq M_{max}$ and $0 \leq n \leq N_{max}$, an approximate version of $f(r,\theta)$, $\hat{f}(r,\theta)$, can be obtained by

$$\hat{f}(r,\theta) = \sum_{n=0}^{N_{max}} \sum_{m=-M_{max}}^{M_{max}} \Phi_{nm} Q_n(r) exp(jm\theta). \tag{7}$$

Although the orthogonal Fourier Mellin moments are defined over the interior of the unit circle, most digital images use the Cartesian image model, which is also adopt in this research. In general, however, implementing a set of circularly defined moments in a Cartesian plane is error prone, especially for the computation related to the pixels along the boundary of unit circle, as shown in Figure 1.

Assuming that the digital image $f(x_i, y_j)$ has the size of $N \times N$, it has been a common practice to replace the orthogonal Fourier Mellin moments defined in (1) with its digital version

$$\widehat{\Phi}_{nm} = \frac{n+1}{\pi} \sum_{i=1}^{N} \sum_{j=1}^{N} f(x_i, y_j) Q_n(r) exp(-jm\theta)\, \Delta x\, \Delta y, \tag{8}$$

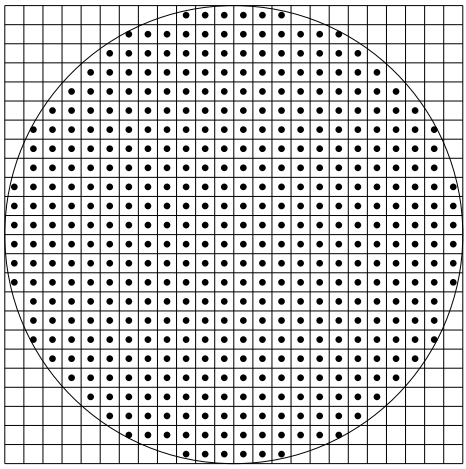

Fig. 1. Image model under the Cartesian coordinate

where Δx and Δy are sampling intervals in the x and y directions, $r = \sqrt{x^2 + y^2}$, and $\theta = \arctan \frac{y}{x}$.

Furthermore, the orthogonal Fourier-Mellin moments Φ_{nm}s in (7) need to be replaced by their digital version expressed in (8), yielding the following basic equation used in the image reconstruction from the orthogonal Fourier-Mellin moments

$$\hat{f}(r,\theta) = \sum_{n=0}^{N_{max}} \sum_{m=-M_{max}}^{M_{max}} \widehat{\Phi}_{nm} Q_n(r) exp(jm\theta). \tag{9}$$

3 Error Analysis of OFMMs Computing

In general, the accuracy of moment computation is an important issue in the field of moment methods, especially for the moments defined in circular domain[9].

Radial and Harmonic Polynomials

For a lower radial order, n, the distribution of $Q_n(r)$ within a pixel is fairly smooth. However, the simulations on $Q_n(r)$ vary significantly when r approaches to 0. Figure 2 shows the distribution of $Q_{60}(r)$ within one of the four central pixels of an image sized 256×256. It indicates that the approximation of $Q_n(r)$ becomes more inaccurate when r approaches 0.

Compared with the radial polynomial, the harmonic basis $exp(-jm\theta)$ turns out to be a more challenging issue for OFMMs computing, especially when the harmonic order, m, goes higher. Figure 3 (a) and (b) illustrate the distributions of real and imaginary parts of $exp(-jm\theta)$, with $m = 60$, in one of the four central pixels of a 256×256 image.

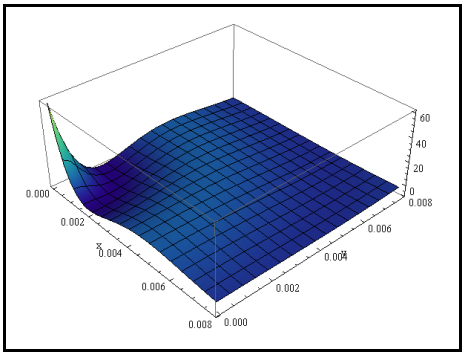

Fig. 2. The distribution of $Q_{60}(r)$ within one of the four central pixels of a 256×256 image

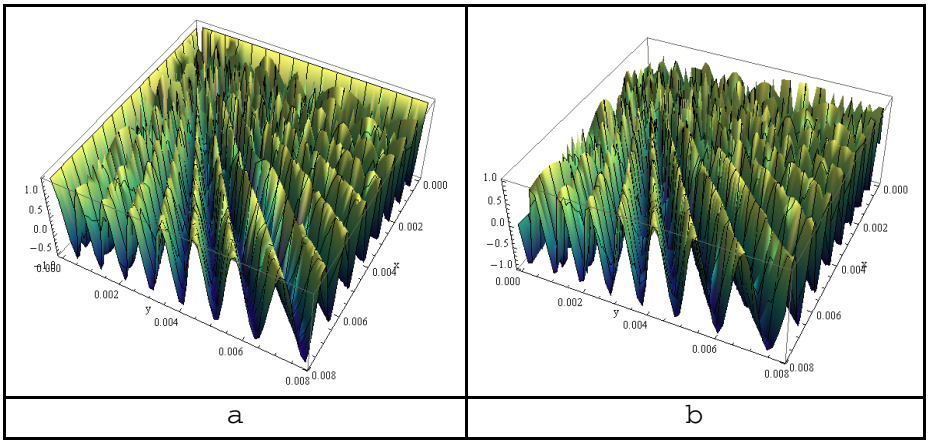

Fig. 3. The distributions of real and imaginary parts of $exp(-jm\theta)$, $m = 60$, within one of the four central pixels of a 256×256 image

Improve the Accuracy of OFMMs

Our analysis of radial and harmonic polynomials concludes that the harmonic polynomial is the major reason that leads to the inaccurate computation of OFMMs. To improve the accuracy of OFMMs computing, we rewrite (8) to

$$\widehat{\Phi}_{nm} = \frac{n+1}{\pi} \sum_{i=1}^{N} \sum_{j=1}^{N} f(x_i, y_j) h_{mn}(x_i, y_j), \tag{10}$$

where

$$h_{mn}(x_i, y_j) = \int_{x_i - \frac{\Delta x}{2}}^{x_i + \frac{\Delta x}{2}} \int_{y_j - \frac{\Delta y}{2}}^{y_j + \frac{\Delta y}{2}} Q_n(r) exp(-jm\theta)\, dxdy. \tag{11}$$

In order to compute the double integrations in (11) accurately, we adopted a new numerical scheme by dividing a pixel into $k \times k$ sub regions with the same weights. By averaging the values of all sub regions, we can considerably reduce the computation errors of both radial and harmonic polynomials.

Geometric error is one of the major computation challenges that affects all image moments defined on a circular domain[6][9][19]. In this research, we take the approach of avoiding all pixels that have a single sub region falling outside the unit circle, other than measuring the centre of each pixel as shown in Figure 1. If the size of an image is $N \times N$, the new radius of our circular domain will be

$$r = 1 - \frac{\sqrt{2}}{N}. \tag{12}$$

This solution can effectively eliminate the geometric error in OFMMs computing with a minimal computation cost.

Image Reconstruction from OFMMs

We would verify our proposed solutions for more accurate OFMMs computation by examining the image reconstruction determined by (9). We have used a 256×256 image with 256 gray levels as our testing image, which is shown in Figure 4.

Fig. 4. The original image with 256 gray levels and a size of 256×256

To compare the reconstructed images with the original testing image, we have adopted the Peak Signal to Noise Ratio (PSNR) as the measurement in this research. PSNR is the ratio between the maximum power of the signal and the affecting noise. For an image $f(x, y)$ with 256 gray levels, the maximum power is 255, and PSNR is defined in decibel (dB) form as

$$PSNR = 10 \log_{10}(\frac{Max^2}{MSE}) = 20 \log_{10} 255 - 10 \log_{10} MSE, \tag{13}$$

where MSE is the Mean Square Error defined as

$$MSE = \frac{1}{N^2} \sum_{i=1}^{N} \sum_{j=1}^{N} [f(x_i, y_j) - \hat{f}(x_i, y_j)]^2 \tag{14}$$

for an original $N \times N$ image $f(x_i, y_j)$ and its reconstructed image $\hat{f}(x_i, y_j)$. The Peak Signal to Noise Ratio is an image independent measurement and can be used to evaluate the reconstruction performance generally. A larger value of PSNR indicates that the reconstructed image is closer to the original one.

We have conducted the image reconstructions from different maximum OFMM orders, with $n = m$, and numerical integration schemes. Table 1 shows the PSNR values resulted from different maximum OFMM orders and $k = 1, 3, 7, 11$, and 15, respectively. Figure 5 shows the images reconstructed from maximum order $n = m = 220$ with different k values, and the original image for comparison.

From Table 1, we observe that the PSNR values are increasing as k increases. Visually, as shown in Figure 5, the improvements on the reconstructed images are more substantial as k increases.

Then, by using the same numerical integration scheme $k = 15$, we have reconstructed images from different maximum radial and harmonic orders. A collection of reconstructed images are displayed in Figure 6.

Table 1. PSNR of different numerical integration scheme k (in dB)

Order(n = m)	10	45	80	115	150	185	220
1×1	21.291	23.357	23.093	21.399	19.166	17.044	15.052
3×3	21.295	23.733	25.186	26.380	27.463	27.847	27.535
7×7	21.295	23.763	25.308	26.779	28.352	30.053	31.883
11×11	21.295	23.767	25.317	26.801	28.461	30.327	32.489
15×15	21.295	23.766	25.323	26.803	28.473	30.352	32.710

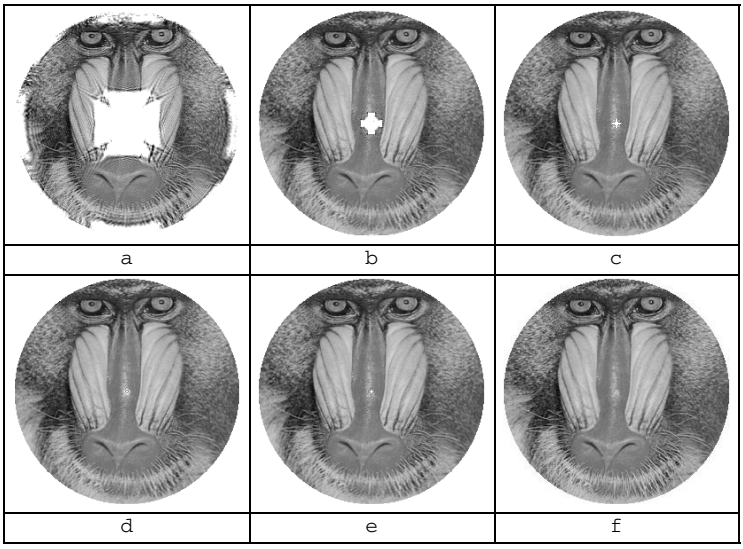

Fig. 5. Sub-figures (a) to (e) are the reconstructed images from orders $n = m = 220$ with the numerical integration scheme of $k = 1, 3, 7, 11$, and 15, respectively. The sub-figure (f) shows the original image for comparison.

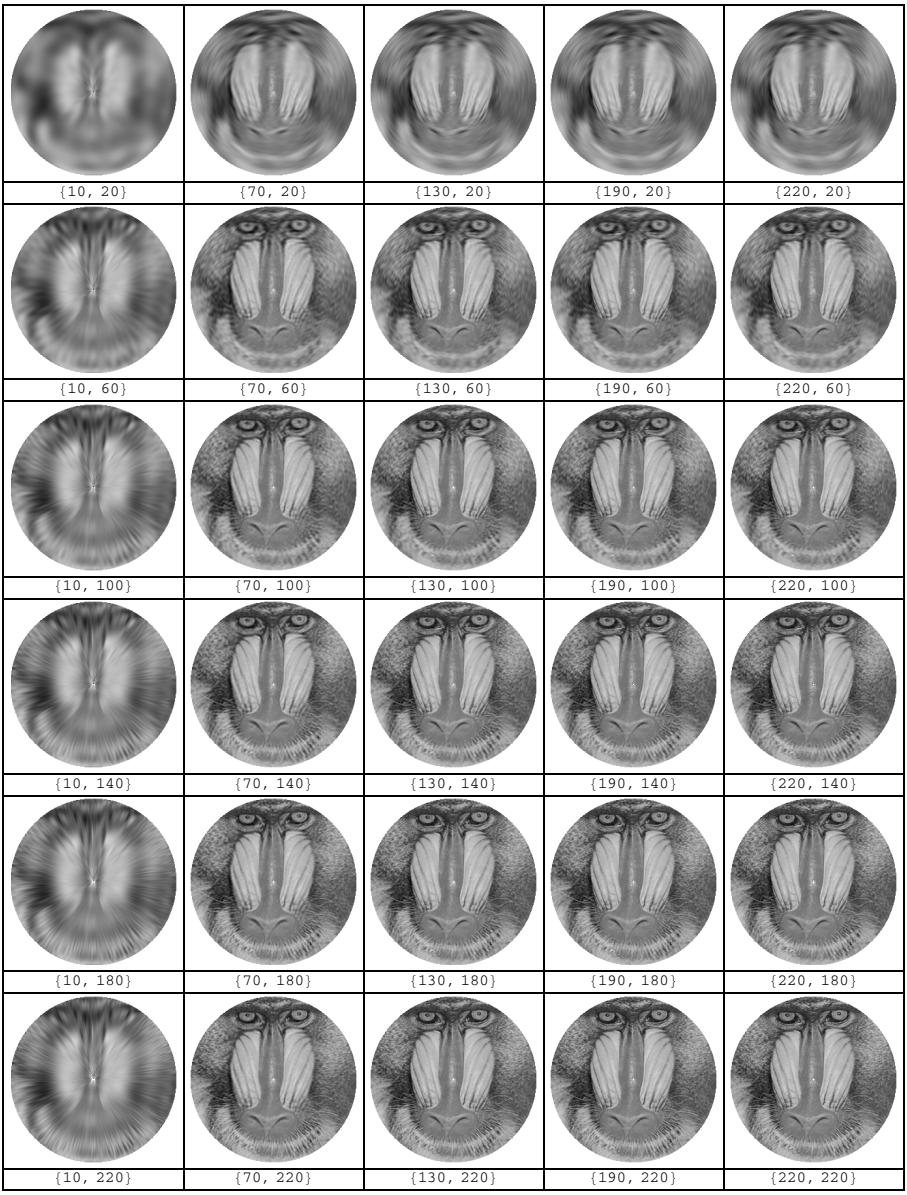

Fig. 6. Reconstructed images from $m = 20, 60, 100, 140, 180, 220$ vertically and $n = 10, 70, 130, 160, 220$ horizontally

4 Concluding Remarks

In this research, we have analyzed the the computation errors related to orthogonal Fourier-Mellin moments computing. To improve the accuracy of OFMMs

computing, a numerical integration method under the Cartesian coordinate system is proposed. To demonstrate the more precisely computed OFMMs, the image reconstructions from higher orders of moments, up to 220 for both of radial and harmonic orders, are examined with satisfied performance.

Based on the accurately computed results, we expect more research progress on investigating of orthogonal Fourier-Mellin moments will be conducted.

References

1. Flusser, J., Suk, T., Zitova, B.: Moments and moment invariants in pattern recognition. John Wiley & Sons, Ltd. (2009)
2. Fu, B., Zhou, J., Li, Y., Peng, B., Liu, L., Wen, J.: Novel recursive and symmetric algorithm of computing two kinds of orthogonal radial moments. Image Science Journal 56, 333–341 (2008)
3. Hosny, K.M., Shouman, M.A., Salam, H.M.: Fast computation of orthogonal fourier-mellin moments in polar coordinates. J. Real-time Image Proc. (2009)
4. Hu, M.K.: Visual pattern recognition by moment invariants. IRE Transactions on Information Theory 8, 179–187 (1962)
5. Liao, S., Pawlak, M.: On image analysis by moments. IEEE Transaction on Pattern Analysis and Machine Intelligence 18(3), 254–266 (1996)
6. Liao, S., Pawlak, M.: On the accuracy of zernike moments for image analysis. IEEE Transactions on Pattern Analysis and Machine Intelligence 20(12), 1358–1364 (1998)
7. Mukundan, R., Ramakrishnan, K.R.: Moment Functions in Image Analysis - Theory and Applications. World Scientific (1998)
8. Papakostas, G.A., Boutalis, Y.S., Karras, D.A., Mertzios, B.G.: Fast numerically stable computation of orthogonal fourier-mellin moments. IET Computer Vision 1, 11–16 (2007)
9. Pawlak, M., Liao, S.: On the recovery of a funtion on a circular domain. IEEE Transaction on Information Theory 48(10), 2736–2753 (2002)
10. Pawlak, M.: Image Analysis by Moments: Reconstrcution and Aomputational Aspects. Oficyna Wydawnicza Politechniki WrocLawskiej, WrocLaw (2006)
11. Ping, Z., Wu, R., Sheng, Y.: Image description with chebyshev-fourier moments. Opt. Soc. Am. 19(9), 1748–1754 (2002)
12. Sheng, Y., Arsenault, H.: Experiments on pattern recognition using invariant fourier-mellin descriptors. Opt. Soc. Am. 3(6), 771–776 (1986)
13. Sheng, Y., Duvernoy, J.: Circular-fourier-radial-mellin descriptors for pattern recognition. J. Opt. Soc. Am. A 3(6), 885–888 (1986)
14. Sheng, Y., Shen, L.: Orthogonal fourier-mellin moments for invariant pattern recognition. Opt. Soc. Am. 11(6), 1748–1757 (1994)
15. Singh, C., Upneja, R.: Accurate computation of orthogonal fourier-mellin moments. Journal of Mathematical Imaging and Vision (2012)
16. Teh, C.H., Chin, R.T.: On digital approximation of moment in invariants. Computer Vision, Graphics and Image Processing 33(3), 318–326 (1986)
17. Walia, E., Singh, C., Goyal, A.: On the fast computation of orthogonal fourier-mellin moments with improved numerical stability. J. Real-time Image Proc. (2010)
18. Wang, X.: Image analysis by orthogonal fourier-mellin moments. Master's thesis, University of Winnipeg, Winnipeg, Manitoba, Canada, R3B 2E9 (2012)
19. Xin, Y., Pawlak, M., Liao, S.: Accurate computation of zernike moments in polar coordinates. IEEE Transaction on Image Processing 16(2), 581–587 (2007)